Comparative Performance Evaluation of Pixel-Level and Decision-Level Data Fusion of Landsat 8 OLI, Landsat 7 ETM+ and Sentinel-2 MSI for Crop Ensemble Classification

Juliana Useya and Shengbo Chen

***Abstract*—Crops mapping unequivocally becomes a daunting task in humid, tropical, or subtropical regions due to unattainability of adequate cloud-free optical imagery. Objective of this study is to evaluate the comparative performance between decision- and pixel-levels data fusion ensemble classified maps using Landsat 8, Landsat 7, and Sentinel-2 data. This research implements parallel and concatenation approach to ensemble classify the images. The multiclassifier system comprises of Maximum Likelihood, Support Vector Machines, and Spectral Information Divergence as base classifiers. Decision-level fusion is achieved by implementing plurality voting method. Pixel-level fusion is achieved by implementing fusion by mosaicking approach, thus appending cloud-free pixels from either Sentinel-2 or Landsat 7. The comparison is based on the assessment of classification accuracy. Overall accuracy results show that decision-level fusion achieved an accuracy of 85.4%, whereas pixel-level fusion classification attained 82.5%, but their respective kappa coefficients of 0.84 and 0.80 but are not significantly different according to Z-test at $\alpha = 0.05$. F1-score values reveal that decision-level performed better on most individual classes than pixel-level. Regression coefficient between planted areas from both approaches is 0.99. However, Support Vector Machines performed the best of the three classifiers. The conclusion is that both decision-level and pixel-level fusion approaches produced comparable classification results. Therefore, either of the procedures can be adopted in areas with inescapable cloud problems for updating crop inventories and acreage estimation at regional scales. Future work can focus on performing more comparison tests on different areas, run tests using different multiclassifier systems, and use different imagery.**

***Index Terms*—Data fusion, ensemble classifier, multiclassifier system, parallel and concatenation approach, plurality voting.**

Manuscript received February 2, 2018; revised May 15, 2018 and August 26, 2018; accepted September 10, 2018. Date of publication November 9, 2018; date of current version November 27, 2018. This work was supported by the Program for JLU Science and Technology Innovative Research Team (No. 2017TD-26), which is funded by the Fundamental Research Funds for the Central Universities, China, the Plan for Changbai Mountain Scholars of Jilin Province, China (JJLZ[2015]54), and Jilin province and Jilin University co-building project: Application and demonstration of satellite remote sensing in crop planting structure adjustment research. *(Corresponding author: Juliana Useya.)*

The authors are with the Department of Remote Sensing and GIS, College of GeoExploration Science and Technology, Jilin University, Changchun 130026, China (e-mail: julieuseya@yahoo.co.uk; chensb@jlu.edu.cn).

Color versions of one or more of the figures in this paper are available online at http://ieeexplore.ieee.org.

Digital Object Identifier 10.1109/JSTARS.2018.2870650

I. Introduction

FOR a number of years, global food security has been on the vanguard as one of the uttermost pressing developmental targets. According to the FAO, in order to achieve food for all by 2050, food production around the world has to grow by more than 60% [1], [2]. Both public and private organizations bear a huge responsibility to raise food production in a sustainable way [3]. For many developing economies, agriculture is the mainstay contributing significantly to Gross Domestic Product (GDP), food security, direct employment, export earnings, and raw materials for other sectors [4]. Food security is one of the most basic actors of our physical and intellectual wellbeing, hence is a fundamental prerequisite for a healthy, active, and happy life [5].

Dealing with food security requires knowledge about the crop types, the land area that is being planted [6] and acreage estimations. Also the monitoring of crops is of vital importance for food security [7]. Croplands maps have great potential for use in preserving prime agricultural farmland [8].

Agriculture is the backbone of Zimbabwe's economy and underpins the economic, social, and political lives of the majority of the people of Zimbabwe [9]. The Zimbabwean government reintroduced "command agriculture," in 2016/7 farming season, which is a program meant to substitute the existing maize import exercise [10]. At least 2000 farmers are expected to benefit from this agricultural scheme aimed at ensuring food self-sufficiency, hence targeting farmers near water bodies who can plant a minimum of 200 hectares of maize per farmer [10]. For inventory purposes, there is great need to identify the types of crops grown on the different farming lands. Crop identification and mapping is the foundation for crop monitoring using remote sensing and is critical to many applications [11], [12]. In Zimbabwe, it can play a big role in controlling the amount of input support required at a given farmland within a district or province.

Consequently, spatially explicit crop system inventories are lacking, since the only available spatial information about crops is collected during national agricultural censuses and are reported by administrative units [13]. Systematic attempts to map crops from remote sensing data are very limited. According to Hentze *et al.* [14], there is an ostensible lack of spatially explicit methods to produce objective data such as the extent of

agricultural area in Zimbabwe. The major limitation to the utilization of remote sensing technology to produce such crop distribution and croplands maps is the excessive cloud cover problem. There exist previous research done regarding this effect, but they all used high temporal resolution MODIS time series. These include Sibanda and Murwira [15], Maguranyanga and Murwira [16], last but not least Hentze *et al.* [14]. The main limitation of MODIS is its low spatial resolution of 500 m, since most farm sizes are very small and heterogeneous.

Upon using freely available satellite imagery with medium spatial resolution, there is need to first mask out all clouds and shadows. The commonly used technique is to restore the clouded pixels with corresponding cloud-free pixels from a different acquisition date either from the same sensor or a different sensor. The acquisition times of the images have to be as close to each other as possible in order to avoid conceivable land use changes. This is one of the different types of pixel-level image fusion, where different sensor datasets are combined into a single composite image which enables a better understanding of the scene.

Image data fusion techniques can be classified into three main categories depending on the stage at which the fusion takes place. These three levels are namely pixel/observation level, feature level, and decision-level of representation [17]–[20]. Schmitt and Zhu [20] provided a holistic view of generic data fusion concepts and their applicability to the remote sensing domain. Wang *et al.* [21] presented a new approach for the fusion of Landsat 8 OLI and Sentinel-2 MSI data in order to coordinate their spatial resolutions for continuous global monitoring.

Major challenges arise when working on areas in the humid, tropical, or subtropical regions where cloud-free data acquisition for a single date is difficult or impossible [22], [23], use of imagery from another sensor becomes apparent. Pixel-level fusion requires knowledge of spectral configurations of the sensors involved, but decision-level does not require knowledge about the spectral bands prior to fusion process. Since cloud masking introduces huge missing data gaps, decision-level fusion is being tested whether it can be an alternative method to the pixel-level fusion. The innovation of this research is to merge classified images (at decision-level) from different image sources with missing data into a seamless classified map. If classification results are accurate enough, then this procedure may contribute to efficiently designing and updating crop inventories [24], for areas in tropical, subtropical, and humid regions which experience inescapable cloud problems.

The general objective of this research is to evaluate the comparative performance between decision-level and pixel-level, seamless crop distribution ensemble classified maps synthesized from integrating Landsat 8, Landsat 7, and Sentinel-2 data. Specific subobjectives of this research are to 1) design and optimize classification schema to conduct ensemble classification using Landsat 8, Landsat 7, and Sentinel-2 data, 2) assess performance of classifiers in multiclassifier systems of the different remotely sensed images, and 3) assess performance of decision-level and pixel-level data fusions.

II. Multiclassifier System

Image classification has made great progress over the past decades, researchers have developed advanced classification approaches and techniques endeavoring to improve classification accuracy, but still classification remain a challenge [25]. Depending on the distribution of patterns, when an individual classifier is trained on a labeled dataset [26], it is possible that not all the patterns are learned well by individual classifiers. However, a solution to such a problem is to train a group of classifiers on the same problem since classifiers can be assumed to have complementary capabilities [27], [28].

The method of combining classifiers can be referred to using different names; including, ensemble classifiers, multiclassifier systems, consensus theory, mixtures of experts, committees of learners [29], [30] but they all refer to a group of individual classifiers that are cooperatively trained on dataset in a supervised classification problem [26]. Ensemble classifier is supposed to perform better than its base counterparts, only if the classifiers are accurate and diverse [26], [31]–[33]. Diversity of an ensemble system determines the success of the classification by correcting the errors of some of its members [33]. Though Kuncheva and Whitaker [29] argued that although there are special cases where diversity and accuracy are connected, their research results do not emphasize on the usefulness of diversity in building classifiers ensembles. There are various approaches of forming a multiclassifier system and it is crucial to choose the best fusion method in order to achieve higher accuracy.

These individual classifiers can be amassed either as 1) cascaded, 2) parallel, or 3) hierarchical configurations [31], [34], [35]. Ranawana and Palade [31] described in detail the criteria to consider when selecting the best topology depending on the type of problem at hand.

There are three properties namely orthogonality, complementarity, and independence to be considered when constructing multiclassifier systems [31], [37]. Orthogonality is not directly measurable but is a rough measurement of how different the decisions are among the different classifiers. The complementarity measures the differences between the strengths and weaknesses of the different classifiers. Independence among classifiers measures the influence that one classifier has over another, over the decision making process, or how results between two classifiers are interrelated [36].

A data/information fusion method (decision-level) combines the decisions produced by the base classifiers. The fusion can lead to improved classification decision compared to a decision based on any of the individual data sources [33]. There exist a good number of fusion methods in literature including; majority voting, Borda count, algebraic combiners [26], decision templates, the Dempster-Shafer based fusion [33], etc. Le Hegarat-Mascle *et al.* [38] successfully applied the Dempster–Shafer Evidence Theory to merge data from unsupervised classification of TMS and AirSAR L and C band images. Ranawana and Palade [31] categorized the fusion methods by classifying them as linear, nonlinear, statistical, and computationally intelligent.

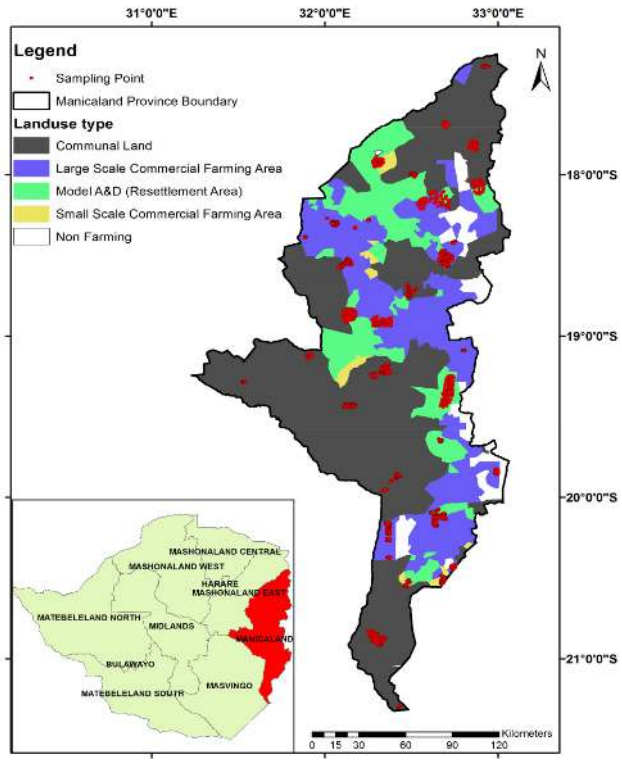

Fig. 1. Study area showing distribution of land use classes and sampling points. Inset shows location of study area (Manicaland province) in Zimbabwe.

Respectfully, majority of research done on multiclassifier system in literature reveal evidence of an improvement made to classification problems due to integration of classifiers. These include Pal [32], Zhang *et al.* [39], Wang *et al.* [40], Kanellopoulos *et al.* [41], Lu [28], last but not least Ho *et al.* [42].

III. Materials

A. Study Area

The study area is Manicaland, located in the eastern province in Zimbabwe that lies between latitude 17°15'00"S and 21°19'12"S, then longitude 31°13'01"E and 33°04'12"E. The province is bounded by Mashonaland East Province to the north, the Republic of Mozambique to the east, Midlands Province to the west, then Masvingo Province to the south and southwest. It covers an area of approximately 36 459 km^2 and four main agricultural land use classes namely communal land, resettlement area, large scale commercial, and small-scale commercial farming areas (see Fig. 1).

Zimbabwe generally has a tropical climate that is dependent on the rains brought by Indian Ocean monsoons (seasonal winds) [9] and has two distinct seasons; summer and winter. Summer crop growing season typically commences in October until March [43]. The summer crops commonly grown include maize, beans, tobacco, sorghum, millet, cotton, groundnuts etc. In February, most summer crops would have reached the peak of the growing season since they are planted either in November/December or January depending on the time of rain onset.

TABLE I
Acquisition Dates of Landsat 8, Sentinel-2, and Landsat 7 Scenes

Landsat 8			Landsat 7			Sentinel-2	
Path	Row	Acquisition Date	Path	Row	Acquisition Date	Product	Acquisition Date
168	72	15 March	168	73	19 February	T36KUE	13 March
168	73	15 March	168	74	19 February	T36KUF	13 March
168	74	15 March	168	75	19 February	T36KVE	8 February
168	75	15 March				T36KVF	30 March
169	72	6 March					
169	73	2 February	169	73	30 March		
169	74	18 February	169	74	26 February		

Dry season starts in April up until September, winter is experienced in June and July. Wheat is the main winter crop planted. However, most of perennial and permanent crops found in Zimbabwe are grown in Manicaland province. These include sugarcane, banana, coffee, tea, etc.

B. Field Data

Training and validation data were collected during different field data campaigns for different purposes from December 2016 until March 2017. A total of 34 500 sampling points were randomly selected and collected (see Fig. 1) using handheld GPS receivers (Trimble Juno 5d, Garmin *e*trex Vista, *e*trex 10, and *e*trex 20). UTM/WGS84 projection coordinate system was adopted during the acquisition. Out of the total points, 22 000 points were used during the class identification process, 12 500 points were used for accuracy assessment.

C. Data Acquisition

Since spectral signatures are associated with phenological stages rather than imaging dates, 2017 February/March imagery for Landsat 8, Landsat 7, and Sentinel-2 with cloud cover not more than 50% were downloaded from a website with this link https://earthexplorer.usgs.gov/.

Both Landsat and Sentinel use the same geographic coordinate system which is Universal Transverse Mercator (UTM) zone 36 South, WGS84 datum. The availability of the three sensors provide the scientific community with a wide range of spatial, spectral, and temporal properties [44]. Table I shows the acquired scenes that were employed in this research and their respective dates when they were acquired. Level-1 Landsat 8 and 7 scenes are downloaded, whereas Sentinel-2 scenes are Level 1C.

IV. Methodology

A. Proposed Schema for Pixel-Level Fusion and Decision-Level Fusion Systems

Fig. 2 presents simple generic flowcharts for pixel-level fusion (left side) and decision-level fusion (right side) systems designed and adopted in this paper. Pixel fusion is performed at an earlier stage than decision-level fusion. Downloaded images are preprocessed prior to the ensemble classification. The classification accuracy assessment results from the two integration methods are compared. All processes are explained in detail in the sections that follow.

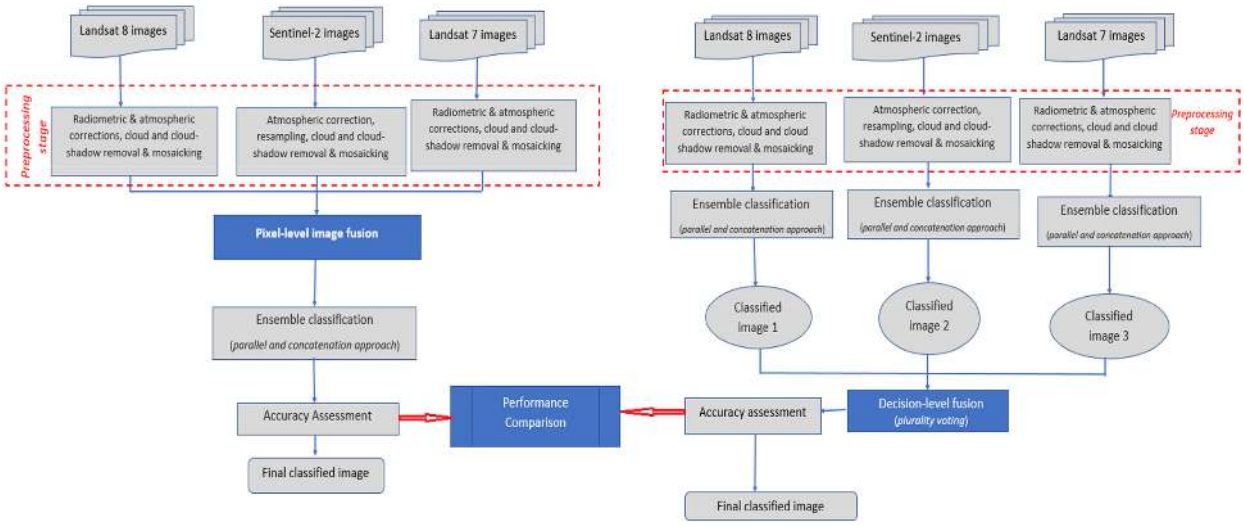

Fig. 2. Generic flowcharts for comparison between pixel-level (left side) and decision-level (right side) fusion processes.

B. Preprocessing

1) Landsat 8 OLI: The downloaded tiles of Landsat 8 OLI are radiometrically corrected. Cloud and cloud shadow removal is implemented using the Fmask algorithm developed and improved by Zhu *et al.* [45], also available in ENVI [46]. Atmospheric correction is applied using QUick Atmospheric Correction (QUAC) module. Cloud-free scenes are later mosaicked and masking is done to exclude areas reserved for wildlife national parks, safari, forests, and urban areas using 2015 land-use shapefile from Surveyor General's office in Zimbabwe.

2) Sentinel-2 MSI: Sentinel-2 mission provides a combination of two satellites namely; Sentinel-2A and Sentinel-2B, hence having a temporal resolution of 5 days at the equator in cloud-free conditions. The Sentinel-2 Level-1C downloaded scenes, only four were usable with cloud cover less than 50%. Level-1C scenes are first converted to top of canopy using Sen2cor atmospheric correction module in SNAP before geometric resampling. All the bands are geometrically resampled to 20 m spatial resolution. 20 m spatial resolution is chosen to preserve and maintain the red-edge bands.

Cloud and cloud-shadow removal is performed in ENVI using method of (ready-to-use) decision tree of depth three as presented by Hollstein *et al.* [47]. Cloud-free images are mosaicked and reserved areas where agriculture is not expected to take place are masked out using 2015 land-use shapefile.

For pixel-level fusion, B2, B3, B4, B8, B11, and B12 are further resampled to 30 m in ArcGIS. For decision-level fusion, base classification of Sentinel-2 are done on B2, B3, B4, B5, B6, B7, B8, B8a, B11, and B12 (at 20 m resolution).

3) Landsat 7 ETM+: Radiometric correction is applied on the downloaded tiles. Gap filling functionality is applied, then cloud and shadow removal is done using Fmask algorithm [45], [46]. Atmospheric correction is applied using QUick Atmospheric Correction (QUAC) module. Cloud-free tiles are then mosaicked. 2015 land-use shapefile from the Surveyor General's office in Zimbabwe was used to mask out areas reserved for national parks and cities. The images are eventually mosaicked, hence ready for pixel-level merging and ensemble classification.

TABLE II
CORRESPONDING SPECTRAL BANDS OF LANDSAT 8, SENTINEL-2, AND LANDSAT 7 USED FOR PIXEL-BASED FUSION

Landsat 8			Sentinel-2			Landsat 7		
Band number	Wavelength (μm)	Spatial resolution (m)	Band number	Wavelength (μm)	Spatial resolution (m)	Band number	Wavelength (μm)	Spatial resolution (m)
2	0.45 – 0.52	30	2	0.46 - 0.52	10	1	0.45 - 0.52	30
3	0.53 – 0.60	30	3	0.54 - 0.58	10	2	0.52 - 0.60	30
4	0.63 – 0.68	30	4	0.65 - 0.68	10	3	0.63 - 0.69	30
5	0.85 – 0.89	30	8	0.79 – 0.90	10	4	0.77 - 0.90	30
6	1.56 -1.66	30	11	1.57 – 1.66	20	5	1.55 - 1.75	30
7	2.10 -2.30	30	12	2.10 – 2.28	20	7	2.09 - 0.35	30

C. Fusion of Raw Data (Pixel-Level Integration)

According to Schmitt and Zhu [20], complementary integration is the fusion of homogeneous sensor data with different information content to reduce information gaps. The combination of sensors with different but complementary measurement ranges, e.g., images with different cloud coverage or complementary spectral ranges is crucial to create a single composite image. Resampling process is implemented in order to achieve data matching or co-registration, which may be necessary not only for the spatial domain.

Mandanici and Bitelli [48] did a preliminary study on the comparison of Sentinel-2 and Landsat 8 imagery for a potential combined use and their results revealed that the corresponding Sentinel-2 and Landsat 8 bands have a very high correlation of their relative spectral response functions (RSRFs), therefore, the pixel-level fusion between the two sensor is justified. Although the RSRFs of the instruments are not identical, some differences are expected in the recorded radiometric values.

For this study, total number of Landsat 8 scenes are more than those of either Landsat 7 or Sentinel-2 tiles, automatically Landsat 8 becomes the target image, while both Landsat 7 and Sentinel-2 are employed as reference images. Jin *et al.* [49] defined in detail the meanings of both target and reference images. However, it is crucial to note that the spectral bands of Sentinel are thinner than Landsat ones. Table II illustrates corresponding spectral bands used in the pixel-level fusion process.

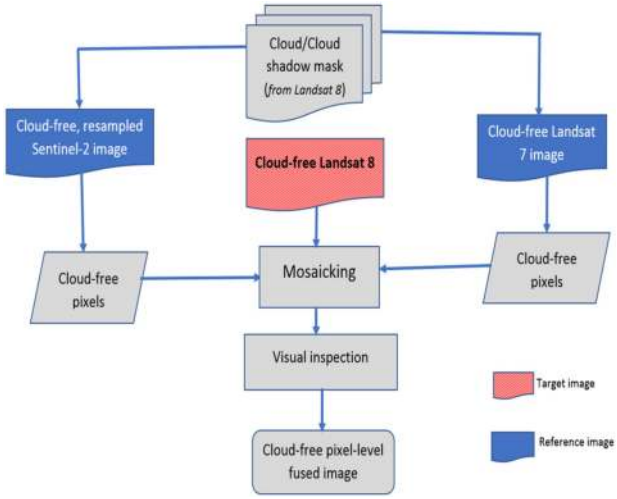

Fig. 3. Flowchart for pixel-level fusion by mosaicking process.

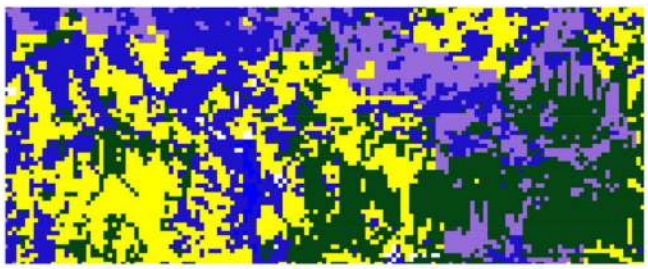

Fig. 4. Cloud-free pixels fusion by mosaicking from Landsat and Sentinel-2.

Fig. 3 illustrates the methodology followed to execute the pixel-level integration. Cloud and cloud shadow mask from Landsat 8 imagery are used to mask out cloud-free pixels from either reference images.

Landsat 7 and 8 have similar spatial resolution of 30 m, whereas the mosaicked Sentinel-2 data (20 m spatial resolution) are further resampled to 30 m using nearest neighbor resampling technique prior to fusion. Cloud-free Sentinel-2 and Landsat 7 pixels are introduced to areas of no information on the Landsat 8 dataset. The fusion is achieved through creating mosaics [17]. Once the cloud/shadow (Landsat 8) and layover/shadow masks (Landsat 7 and Sentinel-2) have been produced, then fusion is performed.

Quality of fused image is assessed by visual means, and Fig. 4 exhibits a sample of the mosaic between Landsat and Sentinel-2. Yellow pixels are from Sentinel-2 which replaced the eliminated clouded pixels from Landsat imagery.

However, there exists a general rule of thumb that says prior to fusing the images, it is crucial to first produce the best single-sensor geometry and radiometry (geocoding, filter, line, edge detection, etc.) and then fuse the images. Any spatial enhancement performed prior to image fusion will benefit the resulting fused images [17]. Fig. 5 shows the mosaicked (processed) images without cloud cover for Landsat 8, Sentinel-2, Landsat 7, and pixel-level fused raw image. The white gaps indicate lack of data and reserved areas as indicated in Fig. 1.

D. Assessment of Training Data Quality

In order to achieve good supervised classification accuracy, the training data need to be of good quality. Therefore, it is crucial to carry out an inspection before performing the classification since the data used for this research was gathered from various researchers.

Rule of thumb states that; it is fundamental to have more training points than the number of spectral bands (i.e., dimensionality). There are three common methods utilized to solve this task namely: 1) visual analysis of the brightness histograms of training areas, 2) visual analysis of training areas' location in the n-Dimension scatter plot, and 3) quantitative evaluation of spectral separability [50].

This research implements Transformed Divergence (TD) and Jeffries-Matusita Distance (JMD). The TD separability measure yields real values between 0 and 2, where 0 indicates complete overlap between the signatures of two classes and 2 indicates a complete separation between the two classes. Divergence measures are related to classification accuracies. The larger the separability values are, the better the final classification results will be. The following rules are suggested for each of the possible ranges of separability values x:

$$\begin{aligned} 0.0 &< \mathbf{x} < 1.0 \ (poor\ separability)\,, \\ 1.0 &< \mathbf{x} < 1.9 \ (moderate\ separability)\,, \\ 1.9 &< \mathbf{x} < 2.0 \ (good\ separability)\,. \end{aligned}$$

In ENVI the Jeffries–Matusita distance is squared to range between 0 and 2, consequently one should take the square root of this output.

According to Apan *et al.* [55], accurate mapping at crop species level is possible when the following ideal conditions are met:

1) the study area is limited to a relatively small region where bio-physical conditions (mainly soil, water regimes, and topography) are homogenous.
2) The study area contains no crops planted at significantly different planting dates.

Literally, these two conditions are rare in nature and perhaps could only be found on experimental plots, or when the focus of the study is on within-field variability mapping. Spectral separability distances are expected to be correlated with classification results, where higher degree of spectra overlapping on the data can lead to poorer accuracy despite the number of bands available.

E. Ensemble Classification

This research implements the parallel and concatenation approach (see Fig. 6) where the classification results generated by individual classifiers are used as an input into the succeeding classifier [36], [51]. Thus, the results obtained through each classifier are similarly passed onto the next classifier until a result is obtained through the final classifier in the chain [51]. Ensemble classifier comprises of MLC, Support Vector Machine (SVM), and Spectral Information Divergence (SID). Classification is

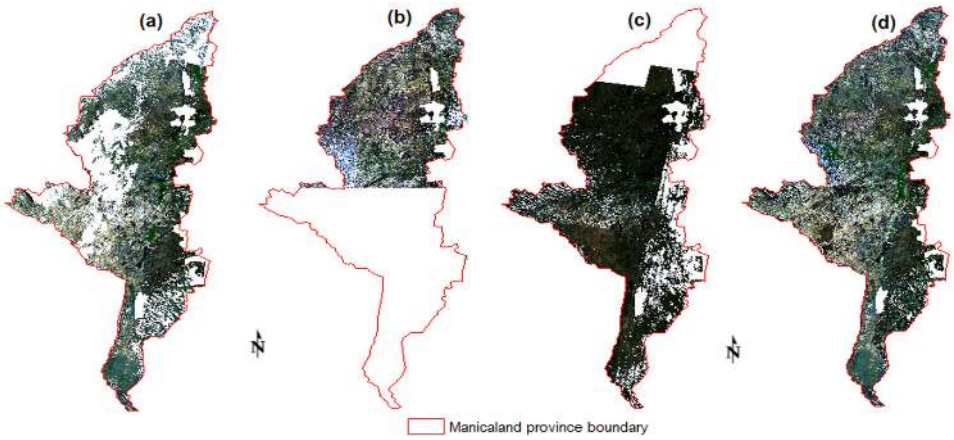

Fig. 5. Mosaicked raw images without clouds. (a) Landsat 8. (b) Sentinel-2. (c) Landsat 7. (d) Pixel-level fused image.

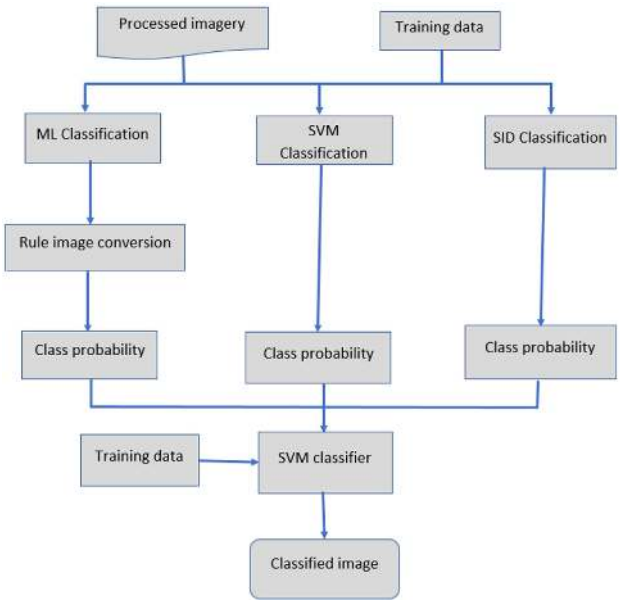

Fig. 6. Flowchart of ensemble classification. Source [51].

done on Landsat 8 OLI images, Sentinel-2 MSI, and Landsat 7 ETM+ independently.

There are several classes to be discerned in the research area, which can be referred to as basic propositions. The probability of the occurrence of one of these propositions, for one sensor, is calculated by summing the probability masses for general propositions that support the occurrence of that basic proposition.

Unification of the base classifiers is done by manipulating the class probabilities for each classifier. The class membership probability images produced from the classification are then reclassified using SVM to integrate the base classifiers. SVM classifier is selected as the second classifier for the reason that it possesses satisfactory capability to deal with the classification problem. This methodology is adopted and modified from Du *et al.* [51] (see Fig. 6). Second classification is performed on *a posteriori* class membership probability images representing the mass probability of a pixel belonging to a class. *A posteriori* class membership probabilities can be denoted by $\Pr(k \mid g)$

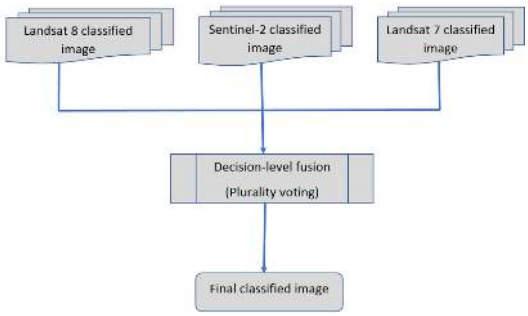

Fig. 7. Flowchart of decision-level fusion.

where g is in class k provided $\Pr(k|g) \geq 1 - \Pr(j|g)$ for all $j = 1 \ldots K$.

But for MLC, in ENVI the rule image produced upon classification, needs to be converted to class membership probability using an IDL code presented by Canty [52], [53] under the assumption that there is no "unclassified" class.

F. Plurality Voting (Decision-Level Fusion)

Where two or more maps overlay, plurality voting [39], [54] is used to decide on the class to be incorporated into the seamless final map. Fig. 7 is a flowchart illustrating the process of decision-level fusion. Classified images from Landsat 8, Sntinel-2, and Landsat 7 are harmonized into a single final classified map. The plurality voting method is the simplest of all combinatorial functions. It selects the relevant class by polling all the classifiers to see which class is the most popular. Whichever class gets the highest vote is selected. This method is particularly successful when the classifiers involved output binary votes.

> "Thus by considering three classifiers: {C1, C2, C3}. Letting x be a new input example. If the three classifiers are absolutely identical, then when C1(x) provides a wrong classification, C2(x) and C3(x) will also provide erroneous results. If the errors made by the three classifiers are uncorrelated, the case might be that when C1(x) is wrong, C2(x) and C3(x) may be correct. In such a case, the majority vote among the three classifiers will correctly classify x." Where the three classes C1(x), C2(x), and C3(x) are different, SVM is used to reclassify them, else choose class with highest correctly classified pixels.

TABLE III
CLASSIFICATION ACCURACIES OF LANDSAT 8, SENTINEL-2, LANDSAT 7, AND FUSED IMAGES

Classifier	Landsat 8	Kappa coefficient	Sentinel-2	Kappa coefficient	Landsat 7	Kappa coefficient	Pixel-level image	Kappa coefficient	Decision-level image	Kappa coefficient
MLC	73.29%	0.71	88.52%	0.88	63.76%	0.59	77.46%	0.75		
SVM	75.37%	0.73	93.63%	0.93	67.56%	0.65	78.58%	0.76		
SID	59.02%	0.54	54.98%	0.53	54.84%	0.49	55.45%	0.53		
MLC + SVM	78.16%	0.75	94.99%	0.94	69.69%	0.67	81.15%	0.79		
SVM + SID	75.47%	0.72	94.50%	0.93	67.78%	0.65	79.85%	0.77		
MLC + SID	73.96%	0.71	89.31%	0.89	63.92%	0.59	77.99%	0.75		
MLV + SVM + SID	78.62%	0.76	96.15%	0.95	69.87%	0.67	**82.52%**	**0.80**	**85.44%**	**0.84**

Preliminary ensemble classified images of Landsat 8 and Landsat 7 are integrated more easily since their spatial resolution is the same (30 m). Sentinel-2 is first resampled to a spatial resolution of 30 m using nearest neighbor technique in ArcMap. Decision-level fusion is eventually performed on Landsat 7, 8, and Sentinel-2 images with same spatial resolution and accurately aligned.

G. Comparison of Classification Results

Based on confusion matrices, overall accuracies are compared. Statistical significance of kappa coefficients is determined using Z-test. Composite measure of producer's and user's accuracies (F1-score) are calculated for each class for comparison of the two fusion methods.

Planted areas from pixel-level and decision-level classification results are compared and a regression line is plotted to determine the relationship between both results.

V. RESULTS

A. Overall Classification Accuracies

Overall statistical accuracies and kappa coefficients obtained from the confusion matrices are used to analyze the quality of classified data obtained from the three individual base classifiers and combinations of integrated classifications results are illustrated by Table III. Kappa coefficient considers the whole error matrix instead of the diagonal elements which is the case with overall accuracy.

SVM outperformed all the base classifiers on all the four datasets classified. It performed the best on Sentinel-2 images achieving an accuracy of 93.63%, followed by 78.58% on pixel-level fused image. MLC achieved 88.52% on Sentinel-2 dataset followed by 77.46% on pixel-level fused image. However, SVM performed slightly better than MLC on all the datasets. It has proved to be a powerful tool for discriminating the various major crops grown in summer using remote sensing. According to Zhang *et al.* [56] and Szuster *et al.* [57], SVM usually yields slightly better results than MLC for land cover analysis. The same has been proved by this research. SID is the least performer but performed fairly well having overall accuracy values between 53–60%.

Endeavoring to improve accuracy of the overall classification, the base classifiers are combined using the base classifiers' *a posteriori* class membership probabilities which were further classified using SVM. In all datasets configurations implemented, the highest accuracy has been achieved by combining the 3 classifiers (MLC + SVM + SID) in all scenarios.

Combining MLC + SVM improves the overall accuracy values but are slightly lower than MLC + SVM + SID. Despite the fact that SID has the lowest accuracy, when combined with either MLC or SVM, it makes a difference, there is a slight increase effected on the ultimate overall accuracy although the magnitude of improvement is small. Generally, the ensemble classifier accomplished better results than its base counterparts. This experiment conducted exploits the idea that diverse classifiers perform differently, even though same training data is used. However, they can provide complementary information about patterns to be determined, thereby increasing the effectiveness of the overall recognition process.

Classifying the fused single composite raw image achieved an accuracy of 82.53% and kappa coefficient of 0.80, whereas the integration of MLC + SVM + SID classified thematic maps from Landsat 8, Landsat 7, and Sentinel-2 achieved an overall accuracy of 85.44% with kappa coefficient of 0.84.

Decision-level fused map attained a better result than pixel-level thematic map. The overall accuracy results prove that decision-level data fusion enable better crops identification compared to classifying a single composite pixel-level integrated image. This indicates that data fusion at decision-level does not lead to any significant data loss, instead there is an improvement in the overall classification accuracy.

B. Statistical Significance of Kappa Coefficients

The Z-test is a statistical test of the difference in accuracy values; it involves comparing the accuracy of a new classifier against one derived from the application of a standard classifier [58]. Z-test is performed to assess significant differences

TABLE IV
Z-TEST STATISTICAL SIGNIFICANCE BETWEEN PIXEL- AND DECISION-LEVEL FUSION RESULTS AT $\alpha = 0.05$

Fusion	Pixel-level	Decision-level
Overall accuracy (%)	82.52	85.44
Kappa $\widehat{K}$	0.80	0.84
$Var\,(\widehat{K})$	0.0056	0.0027
$z = \dfrac{\widehat{K}_1 - \widehat{K}_2}{\sqrt{\sigma^2_{\widehat{K}_1} + \sigma^2_{\widehat{K}_2}}}$	***-0.4391***	
Significance	***Not significant***	

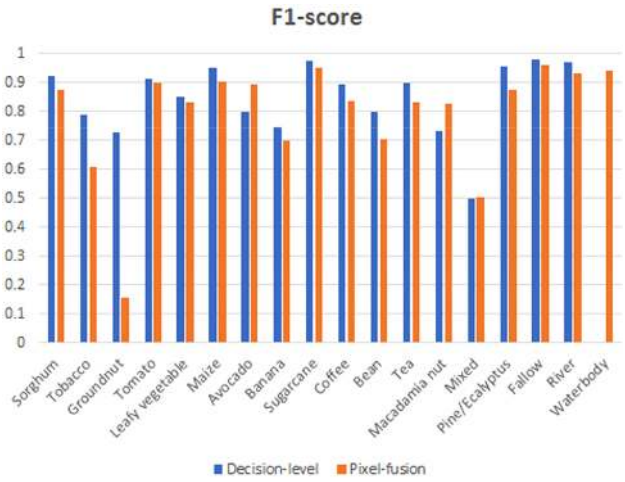

Fig. 8. F1-score values for the different classes discerned in the study.

between the accuracy measurements of classification results [58] from pixel-level and decision-level fusions.

Initial kappa coefficients computed in ENVI, their respective confusion matrices are exported to MATLAB to obtain the variance estimates ($\sigma^2_{\hat{K}_1}$ and $\sigma^2_{\hat{K}_2}$) necessary to compare the different tests. Table IV exhibits the result for the computed z-value of -0.4391, indicating that there is a no significant difference between the kappa values at $\alpha = 0.05$.

C. Classification Performance on Individual Classes

Individual class accuracies from decision-level and pixel-level approaches are assessed in this section by F1-score values calculated from producer's and user's accuracies. Since overall accuracy does not reveal whether error was evenly distributed between classes or if some classes were really bad and some really good, user's and producer's accuracies can be considered.

The higher the F1-score, the better the representation. The best F1-measurement a class can achieve is 1, the worst is 0. Fig. 8 illustrates the F1-scores represented by the bar graph. F1-score represents the mean of precision and sensitivity, that is a composite measure of user's and producer's accuracies are calculated for each class by the following equation:

$$F1\ \text{score} = 2 \times \frac{PA \times UA}{PA + UA}$$

where PA is producer's accuracy whereas UA is user's accuracy.

Decision-level method managed to correctly represent most classes in the thematic map compared to pixel-level based fused thematic map. Exceptions are avocado, macadamia nuts and mixed classes.

D. Crops Distribution Maps

Fig. 9 depicts seamless crops distribution maps synthesized from 1) pixel-level fusion and 2) decision-level fusion approaches. Visually comparing the two summer crops distribution maps, they reveal similar patterns, the differences between these two is minimal and inevitable. This is an indication that the classification processes of the two procedures synthesize almost similar products. Generally, maize is the dominating crop grown in summer.

Fig. 10 displays a sugarcane estate as depicted by classified images from pixel-level and decision-level fusion system. Most of the areas planted the sugarcane look similar between the two images whereas some areas with different classes discerned are visible.

Zimbabwe's Ministry of Agriculture, Mechanization, and Irrigation Development [59] released a report titled "First round crop and livestock assessment (2016–2017)," on the 6th of March with total hectares of areas planted of the different crops in all provinces. Therefore, the areas of crop species in Manicaland province from the report and from this study are compared qualitatively. Generally, for all the crops compared, both fusion approaches produced higher values of total planted areas than those recorded in the first-round assessment report. The relationship between planted areas from the report and decision-level produced $R^2 = 0.99$ whereas planted areas recorded in report and pixel-level has $R^2 = 0.99$. Relationship between planted areas from decision-level and pixel-level approaches has a $R^2 = 0.99$.

VI. DISCUSSION

The resultant fused composite image synthesized from synergistic combination of multisource images of a scene can provide more accurate and reliable information about that scene than any individual source images [60], [61]. Due to inescapable cloud cover, image fusion systems provide great practical valuable data and information crop mapping. Furthermore, less costly information may be obtained from a system using multisensor fusion [61].

This research is aimed at evaluating the performance of decision-level and pixel-level fusion methods in an ensemble classifier to determine crops. From the results, decision-level approach achieved 85.4% as compared to 82.5% obtained by pixel-level approach. Respective kappa coefficients are 0.84 and 0.80 but are not significantly different according to Z-statistical test at 95% confidence interval. This means that results from decision-level approach and those from pixel-level at district level are comparable.

Integration systems provide redundant information from the three sensors, hence, fusion of redundant information can reduce overall uncertainty and thus serve to increase accuracy [61]. Moreover, the fusions allow the integration of complementary

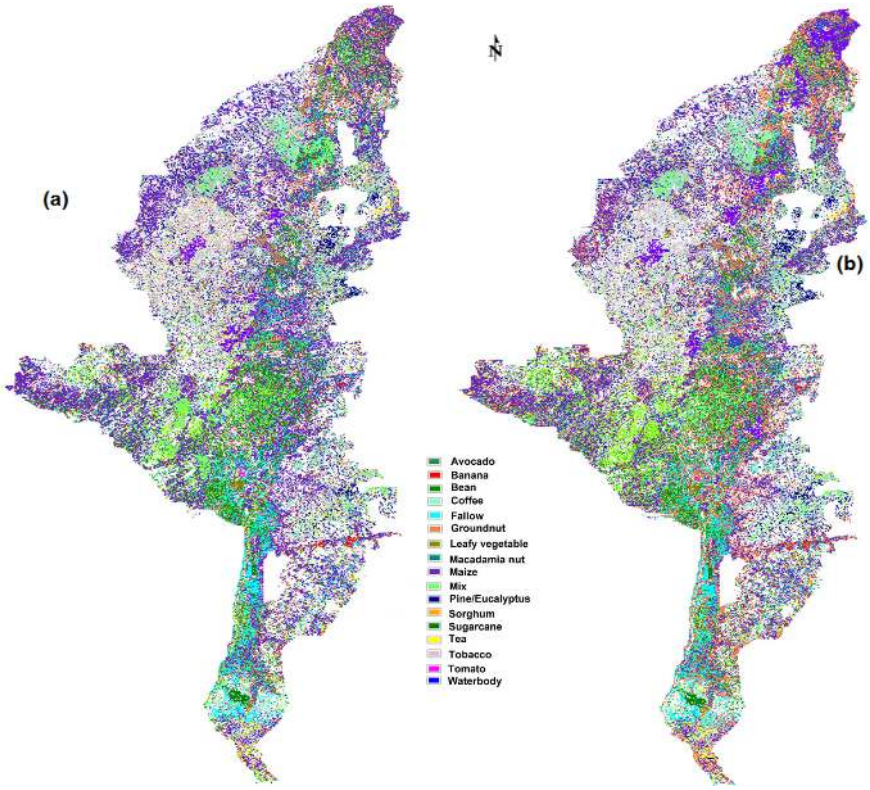

Fig. 9. Classified images. (a) Pixel-level. (b) Decision-level.

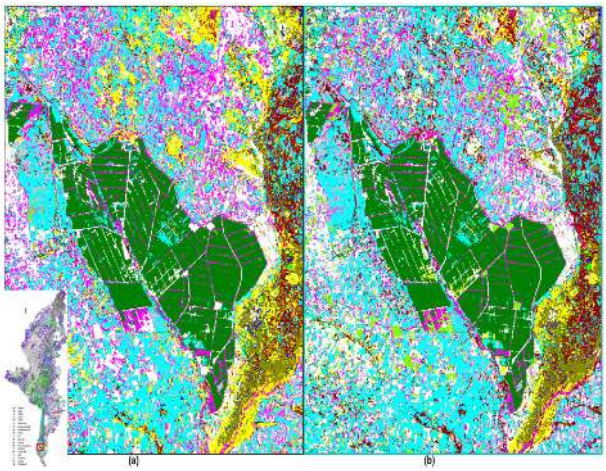

Fig. 10. Sugarcane estate from (a) pixel-level, and (b) decision-level classified maps. Inset shows location of sugarcane estate on classified map marked by red rectangle.

information provided by each sensor concerning a subset of the features in the environment.

Nevertheless, it is indispensable to combine multiple classifiers to yield a better result than any individual classifiers. The advantage of decision-level integration is that all information from each sensor imagery can be applied separately. Classifying Landsat 8 produced comparable results to those of Sentinel-2. The best performance from Sentinel-2 is due to added value to land use mapping that comes along with Sentinel-2 red-edge bands [44]. Sentinel-2 has red edge bands which play a crucial role in vegetation analysis. These red-edge bands are not available in the Landsat spectral configurations. The main disadvantage of Landsat 7, is the scan line corrector failure, hence algorithms employed in filling the gaps will never produce a true representation of the area covered. Gap filling is about 70% effective in regenerating to lost data, of which the lost data is about 22%. In areas where there is less or no cloud cover, multiple acquisitions can be merged to resolve the SLC-off data gaps. Other Landsat 7 users do not apply the gap filling algorithms, since they regard them to be inaccurate. Fused image produced by pixel-level fusion approach is limited to only six bands which do not include the red-edge bands from Sentinel-2.

The other advantage of decision-level fusion is that no prior knowledge about the spectral configuration of the various sensors involved is required. To this fact, it becomes the main limitation of pixel-level fusion. In the event that there is/are no corresponding bands, the restoration of cloud pixels is not possible. Further research is necessary to determine whether decision-level always perform better than pixel-level fusion on different environmental conditions.

The disadvantage of decision-level fusion, nevertheless, is still the limited possibility of decision boundaries, because the operations are restricted to voting/thresholding, AND, and OR [62].

Considering time consumption aspect, pixel-level approach consumes relatively less time than the decision-level approach. Computational costs are the same since freely available satellite images are utilised. Storage space for decision-level fusion procedure is greater than for pixel-level fusion.

It is possible to create reliable seamless crop distribution maps from merging classified images at decision-level using freely available multispectral images with poor data quality coverage. Both fusion systems can be used for crop mapping, and the maps are useful for inventory purposes, and acreage estimation at regional scale using remote sensing. Crop distribution and acreage are crucial for information for good agricultural management and policy making.

Ensemble classifiers reduce the probability of overfitting and bias or variance error, hence exploit the idea that different classifiers can provide complementary information about patterns to be classified, thereby improving the effectiveness of the overall recognition process [30]. SVM classification produced the best classification results basing on the statistical accuracy assessments performed on the Landsat 8, Sentinel-2, and Landsat 7 imagery. Multiclassifier systems are supposed to improve the overall accuracy of classification results. In this paper, MLC + SVM + SID improved classification accuracies of classification on all the three-sensor data. It is higher than SVM classification accuracies on the three datasets. However, it is necessary to determine the optimal size of an ensemble that performs and produces the best results. Further research can be done by creating different ensemble classifiers comprising of different base classifiers and run tests on different imagery, different areas, and compare the two fusion approaches.

VII. Conclusion

This paper evaluated the comparative performance of decision and pixel levels data fusion on ensemble classification using Landsat 8, Landsat 7, and Sentinel-2 data. Overall classification results reveal that decision-level approach attained better accuracy of 85.4% compared to 82.5% achieved by classifying pixel-level fused image. However, their corresponding kappa coefficients of 0.84 and 0.80 are compared statistically using Z-test and reveal that both methods are not significantly different at $\alpha = 0.05$. To accomplish objectives of this research, the first subobjective is to develop a classification schema and has been designed as presented by Fig. 2.

Second subobjective is to assess the performance of base classifiers in the multiclassifier system. Parallel and concatenation approach has been implemented to execute the multiclassifier system. SVM performs the best of the three base classifiers, followed by MLC and lastly SID on all the datasets. Integrating the three (SVM + MLC + SID) achieved the highest accuracy, followed by fusing SVM + MLC on all cases.

The final subobjective is to assess performance of decision-level and pixel-level data fusions. F1-test has been implemented to determine the performance on individual classes, results exhibit that decision-level data fusion performed better in discriminating most classes compared to performance on individual classes from a single composite pixel-level integrated image. The exceptional classes are avocado, macadamia nut, and mixed crops. Regression coefficient (r) between planted areas from pixel-level and decision-level fusion systems is 0.99. Therefore, the performances of the two fusion methods can be concluded to be similar significantly.

Acknowledgment

The authors are very grateful to the following people who availed their GNSS captured field data collected for their own researches in the different parts of Manicaland Province: M. Murefu, L. Buka, A. Chemura, F. Useya, S. Togarepi, M. Chawira, and S. Sigauke.

References

[1] M. Ustuner, M. T. Esetlili, F. B. Sanli, and S. Abdikan, "Comparison of crop classification methods for the sustainable agriculture management," *J. Environ. Prot. Ecol.*, vol. 655, no. 2, pp. 648–655, 2016.
[2] FAO, *Climate-Smart Agriculture Sourcebook*. Rome: FAO, 2013.
[3] Proba-Vegetation, "Agriculture," Belgium, 2017.
[4] D. Kutywawo, A. Chemura, and T. Chagwesha, "Soil quality and cropping patterns as a ffected by iirigation water quality in mutema irrigation," in *Proc. 13th WaterNet / WARFSA / GWP-SA Symp.*, pp. 1–6, Oct. 2012.
[5] B. Wu *et al.*, "Global crop monitoring: A satellite-based hierarchical approach," *Remote Sens.*, vol. 7, no. 4, pp. 3907–3933, Apr. 2015.
[6] M. G. C. Gómez, "Joint use of sentinel-1 and sentinel-2 for land cover classification: A machine learning approach," Lund Univ., Lund, Sweden, 2017.
[7] E. Roumenina *et al.*, "Single- and multi-date crop identification using PROBA-V 100 and 300 m S1 products on zlatia test site, bulgaria," *Remote Sens.*, vol. 7, no. 10, pp. 13843–13862, Oct. 2015.
[8] D. I. M. Enderle and R. C. Weihjr, "Integrating supervised and unsupervised classification methods to develop a more accurate land cover classification," *J. Ark. Acad. Sci.*, vol. 59, pp. 65–73, 2005.
[9] A. A. Maiyaki, "Zimbabwe's agricultural industry," *African J. Bus. Manag. Dec. Spec. Rev.*, vol. 4, no. 19, pp. 4159–4166, 2010.
[10] T. Mutenga, "Command agric misses target," *Financial Gazette*, p. 1, Aug. 2017.
[11] Z. Mingwei, Z. Qingbo, C. Zhongxin, L. Jia, Z. Yong, and C. Chongfa, "Crop discrimination in Northern China with double cropping systems using fourier analysis of time-series MODIS data," *Int. J. Appl. Earth Obs. Geoinf.*, vol. 10, no. 4, pp. 476–485, Dec. 2008.
[12] M. Ustuner, F. B. Sanli, S. Abdikan, M. T. Esetlili, and Y. Kurucu, "Crop type classification using vegetation indices of rapideye imagery," in *Int. Arch. Photogramm. Remote Sens. Spatial Inf. Sci. ISPRS Archives*, vol. 40, no. 7, pp. 195–198, 2014.
[13] A. Mukashema, "Smallholder coffee terroirs of rwanda: Linking local to global trade through geographical characterization," University of Twente, Enschede, The Netherlands, 2017.
[14] K. Hentze, F. Thonfeld, and G. Menz, "Evaluating crop area mapping from MODIS time-series as an assessment tool for zimbabwe's 'fast track land reform programme,' " *PLoS One*, pp. 1–22, 2016.
[15] M. Sibanda and A. Murwira, "The use of multi-temporal MODIS images with ground data to distinguish cotton from maize and sorghum fields in smallholder agricultural landscapes of Southern Africa," *J. Int. Sens. Remote*, vol. 33, no. 16, pp. 4841–4855, Aug. 2012.
[16] C. Maguranyanga and A. Murwira, "Mapping maize, tobacco, and soybean fields in large-scale commercial farms of zimbabwe based on multitemporal NDVI images in MAXENT," *Can. J. Remote Sens.*, vol. 40, no. 6, pp. 396–405, 2015.
[17] C. Pohl and J. L. Van Genderen, "Review article multisensor image fusion in remote sensing: Concepts, methods and applications," *Int. J. Remote Sens.*, vol. 19, no. 5, pp. 823–854, Jan. 1998.
[18] F. A. Al-Wassai, N. V Kalyankar, and A. A. Al-Zuky, "The IHS transformations based image fusion," *Int. J. Glob. Res. Comput. Sci.*, vol. 2, no. 5, pp. 70–77, 2011.
[19] J. Zhang, "Multi-source remote sensing data fusion: Status and trends," *Int. J. Image Data Fusion*, vol. 1, no. 1, pp. 5–24, Mar. 2010.
[20] M. Schmitt and X. X. Zhu, "Data fusion and remote sensing: An evergrowing relationship," *IEEE Geosci. Remote Sens. Mag.*, vol. 4, no. 4, pp. 6–23, Dec. 2016.
[21] Q. Wang *et al.*, "Fusion of landsat 8 OLI and sentinel-2 MSI data," *IEEE Trans. Geosci. Remote Sens.*, vol. 55, no. 7, pp. 3885–3899, Jul. 2017.
[22] S. Martinuzzi, W. A. Gould, and O. M. R. González, "Creating cloud-free landsat ETM+ data sets in tropical landscapes: Cloud and cloud-shadow removal," United States Department of Agriculture, Washington, DC, USA, Tech. Rep. IITF-GTR-32, 2007.
[23] C. Zhu, D. Lu, D. Victoria, and L. V. Dutra, "Mapping fractional cropland distribution in mato grosso, brazil using time series MODIS enhanced vegetation index and landsat thematic mapper data," *Remote Sens. MDPI*, vol. 8, no. 22, pp. 1–14, 2015.

[24] M. A. Peña, R. Liao, and A. Brenning, "Using spectrotemporal indices to improve the fruit-tree crop classification accuracy," *ISPRS J. Photogramm. Remote Sens.*, vol. 128, pp. 158–169, 2017.
[25] D. Lu and Q. Weng, "A survey of image classification methods and techniques for improving classification performance," *Int. J. Remote Sens.*, vol. 28, no. 5, pp. 823–870, Mar. 2007.
[26] A. Rahman and S. Tasnim, "Ensemble classifiers and their applications: A review," *Int. J. Comput. Trends Technol.*, vol. 10, no. 1, pp. 31–35, Apri. 2014.
[27] T. Matsuyama, "Knowledge-based aerial image understanding systems and expert systems for image processing," *IEEE Trans. Geosci. Remote Sens.*, vol. GE-25, no. 3, pp. 305–316, May 1987.
[28] Y. Lu, "Knowledge integration in a multiple classifier system," *Appl. Intell.*, vol. 6, no. 2, pp. 75–86, 1996.
[29] L. I. Kuncheva and C. J. Whitaker, "Measures of diversity in classifier ensembles," *Mach. Learn.*, vol. 51, no. 51, pp. 181–207, 2003.
[30] N. M. Baba, M. Makhtar, S. Abdullah, and M. K. Awang, "Current issues in ensemble methods and its applications," *J. Theoretical Appl. Inf. Technol.*, vol. 81, no. 2, pp. 266–276, 2015.
[31] R. Ranawana and V. Palade, "Multi-classifier systems: Review and a roadmap for developers multi-classifier systems - review and a roadmap for developers," *Int. J. Hybrid Intell. Syst.*, vol. 3, pp. 35–61, 2006.
[32] M. Pal, "Ensemble learning with decision tree for remote sensing classification," *World Acad. Sci. Eng. Technol.*, vol. 36, pp. 258–260, 2007.
[33] R. Polikar, "Ensemble learning," *Scholarpedia*, vol. 1, no. 1, pp. 1–34, 2009.
[34] X. Liu, A. K. Skidmore, H. van Oosten, and H. Heine, "Integrated classification systems," in *Proc. 2nd Int. Symp. Operationalization Remote Sens.*, pp. 16–20, Aug. 1999.
[35] Y. I. Lu, "Knowledge integration in a multiple classifier system," *Appl. Intell.*, vol. 6, no. 2, pp. 75–86, 1996.
[36] R. Ranawana and V. Palade, "Multi-classifier systems: Review and a roadmap for developers multi-classifier systems - review and a roadmap for developers," *Int. J. Hybrid Intell. Syst.*, vol. 3, pp. 35–61, Apr. 2006.
[37] L. Lam, "Classifier combinations: Implementations and theoretical issues," in *Multiple Classifier Systems 2000, Lecture Notes in Computer Science*. vol. 1857, Berlin,Germany: Springer, 2000, pp. 77–86.
[38] S. Le Hegarat-Mascle, I. Bloch, and D. Vidal-Madjar, "Application of dempster-shafer evidence theory to unsupervised classification in multisource remote sensing," *IEEE Trans. Geosci. Remote Sens.*, vol. 35, no. 4, pp. 1018–1031, Jul. 1997.
[39] X. Zhang, X. Feng, and W. Ke, "Integration of classifiers for improvement of vegetation category identification accuracy based on image objects," *New Zealand J. Agricultural Res.*, vol. 50, no. 5, pp. 1125–1133, Dec. 2007.
[40] J. Wang, G. Su, J. Chen, and Y. Moon, "CPGL: A classification method combining PCA and group lasso method," in *Proc. IEEE 17th Int. Conf. Image Process.*, 2010, pp. 4529–4532.
[41] I. Kanellopoulos, G. G. Wilkinson, and J. Megier, "Integration of neural network and statistical image classification for land cover mapping," in *Proc. IEEE Int. Geosci. Remote Sens. Symp*, 1993, pp. 511–513.
[42] T. K. Ho, J. J. Hull, and S. N. Srihari, "Decision combination in multiple classifier systems," *IEEE Trans. Pattern Anal. Mach. Intell.*, vol. 16, no. 1, pp. 66–75, Jan. 1994.
[43] A. Chemura, O. Mutanga, and J. Odindi, "Empirical modeling of leaf chlorophyll content in coffee (coffea arabica) plantations with sentinel-2 MSI data: Effects of spectral settings, spatial resolution, and crop canopy cover," *IEEE J. Sel. Topics Appl. Earth Observ. Remote Sens.*, vol. 10, no. 12, pp. 5541–5550, Dec. 2017.
[44] G. Forkuor, K. Dimobe, I. Serme, and J. E. Tondoh, "Landsat-8 vs. sentinel-2: Examining the added value of sentinel-2's red-edge bands to land-use and land-cover mapping in burkina faso," *GIScience Remote Sens.*, vol. 55, pp. 1–24, Aug. 2017.
[45] Z. Zhu, S. Wang, and C. E. Woodcock, "Remote sensing of environment improvement and expansion of the fmask algorithm: Cloud, cloud shadow, and snow detection for landsats 4–7, 8, and sentinel 2 images," *Remote Sens. Environ.*, vol. 159, pp. 269–277, 2015.
[46] H. G. Solutions, "ENVI calculate cloud mask using fmask task," 2018. [Online]. Available: http://www.harrisgeospatial.com/docs/envicalculatecloudmaskusingfmasktask.html. Accessed on: Apr. 9, 2018.
[47] A. Hollstein, K. Segl, L. Guanter, M. Brell, and M. Enesco, "Ready-to-use methods for the detection of clouds, cirrus, snow, shadow, water and clear sky pixels in sentinel-2 MSI images," *MDPI Remote Sens.*, vol. 8, no. 666, pp. 1–18, 2016.
[48] E. Mandanici and G. Bitelli, "Preliminary comparison of sentinel-2 and landsat 8 imagery for a combined use," *Remote Sens.*, vol. 8, no. 12, p. 1014, 2016.
[49] S. Jin *et al.*, "Automated cloud and shadow detection and filling using two-date Landsat imagery in the USA," *Int. J. Remote Sens.*, vol. 34, no. 5, pp. 1540–1560, Mar. 2013.
[50] P. Ukrainski, "Supervised classification help. ROI separability," *50°North*, 2016. [Online]. Available: 50northspatial.org. Accessed on: Dec. 25, 2017.
[51] P. Du, J. Xia, W. Zhang, K. Tan, Y. Liu, and S. Liu, "Multiple classifier system for remote sensing image classification: A review," *Sensors MDPI*, vol. 12, no. 12, pp. 4764–4792, Apr. 2012.
[52] M. J. Canty, *Image Analysis, Classification And Change Detection In Remote Sensing*, 3rd ed. New York, NY, USA: Taylor & Francis, 2014.
[53] M. J. Canty, *Image Analysis, Classification, and Change Detection in Remote Sensing*, 2nd ed. New York, NY, USA: Taylor & Francis, 2009.
[54] X. Lin, S. Yacoub, J. Burns, and S. Simske, "Performance analysis of pattern classifier combination by plurality voting," *Pattern Recognit. Lett.*, vol. 24, no. 12, pp. 1959–1969, 2003.
[55] A. Apan, R. Kelly, T. Jensen, D. Butler, W. Strong, and B. Basnet, "Spectral discrimination and separability analysis of agricultural crops and soil attributes using aster imagery," in *Proc 11th Australas. Remote Sens. Photogramm. Conf.,* Brisbane, Australia, Jan. 2002, vol. 2, pp. 396–411.
[56] Y. Zhang, J. Ren, and J. Jiang, "Combining MLC and SVM classifiers for learning based decision making: Analysis and evaluations," *Comput. Intell. Neurosci.*, vol. 2015, pp. 1–8, 2015.
[57] B. W. Szuster, Q. Chen, and M. Borger, "A comparison of classification techniques to support land cover and land use analysis in tropical coastal zones," *Appl. Geogr.*, vol. 31, no. 2, pp. 525–532, Apr. 2011.
[58] K. Jia *et al.*, "Land cover classification of landsat data with phenological features extracted from time series MODIS NDVI data," *Remote Sens.*, vol. 6, no. 11, pp. 11518–11532, 2014.
[59] M. of A. M. and I. Development, "First round crop and livestock assessment report (2016–2017)," Harare, Zimbabwe, 2017.
[60] E. Nirmala and V. Vaidehi, "Comparison of pixel-level and feature level image fusion methods," in *Proc. Int. Conf. Comput. Sustain. Global Develop.*, 2015, pp. 743–748.
[61] R. S. Blum, Z. Xue, and Z. Zhang, "An overview of image fusion," in *Multi-Sensor Image Fusion and Its Applications*, R. S. Blum and Z. Liu, Eds. New York, NY, USA: Taylor & Francis, 2006, pp. 2–35.
[62] Q. Tao and R. Veldhuis, "Hybrid fusion for biometrics: Combining score-level and decision-level fusion hybrid fusion for biometrics: Combining score-level and decision-level fusion," in *Proc. IEEE Comput. Soc. Conf. Comput. Vis. Pattern Recognit. Workshops*, no. Jul. 2008.

Juliana Useya received the B.Sc. (Hons.) degree in geoinformatics and surveying from the University of Zimbabwe, Zimbabwe, in 2007, and the M.Sc. degree in geoinformatics from the Faculty of ITC, University of Twente, Enschede, The Netherlands, in 2011. She is currently working toward the Postgraduate degree in the Department of Remote Sensing and GIS at the College of GeoExploration Science and Technology, Jilin University, China.

Her research interests include multisensor classification and synthetic aperture radar application techniques.

Shengbo Chen received the Ph.D. degree in earth exploration and information technology in 2000 from Jilin University, Changchun, China.

He is a full professor at College of GeoExploration Science and Technology, Jilin University, China. His current research interests include application of remote sensing in geology, agriculture, and exploration of the lunar system.